Kobe University Repository : Kernel

PDF issue: 2025-12-04

Magnetic Purcell Enhancement by Magnetic Quadrupole Resonance of Dielectric Nanosphere Antenna

Sugimoto, Hiroshi
Fujii, Minoru

(Citation)
ACS Photonics,8(6):1794-1800

(Issue Date)
2021-06-16

(Resource Type)
journal article

(Version)
Accepted Manuscript

(Rights)
This document is the Accepted Manuscript version of a Published Work that appeared in final form in ACS Photonics, copyright © 2021 American Chemical Society after peer review and technical editing by the publisher. To access the final edited and published work see https://doi.org/10.1021/acsphotonics.1c00375.

(URL)
https://hdl.handle.net/20.500.14094/0100482011

Magnetic Purcell Enhancement by Magnetic Quadrupole Resonance of Dielectric Nanosphere Antenna

Hiroshi Sugimoto,[*,†,‡] and Minoru Fujii*[†]

[†]Department of Electrical and Electronic Engineering, Graduate School of Engineering, Kobe University, Rokkodai, Nada, Kobe 657-8501, Japan

[‡]JST-PRESTO, Honcho 4-1-8, Kawaguchi, Saitama 332-0012, Japan

KEYWORDS : *nanoantenna, Mie resonance, magnetic dipole, europium, silicon, nanoparticles*

ABSTRACT

Dielectric nanoantennas have been suggested for manipulating spontaneous emission of a magnetic dipole through the magnetic Purcell effect. However, the experimentally observed enhancement of magnetic dipole emission has been marginal and much smaller than the theoretical prediction. Here, we develop a composite system, that is, a Si nanosphere decorated with Eu^{3+} complexes, in which magnetic dipole emission of Eu^{3+} is efficiently coupled to the magnetic Mie modes of the nanosphere. By means of single particle spectroscopy, we systematically investigate the light scattering and photoluminescence spectra of the coupled system with diameters of Si nanospheres from 130 to 245 nm. We demonstrate that by tuning the magnetic quadrupole Mie resonance to the $^5D_0$-$^7F_1$ magnetic dipole transition of Eu^{3+}, the branching ratio between the magnetic and electric dipole transitions is enhanced up to 7 times. We also show the magnetic Purcell enhancement in an ensemble of Si nanospheres with size distribution.

Optical nanoantennas play a central role for enhanced light-matter interactions in modern nanophotonics.[1,2] Integration of a quantum emitter into a nanoantenna that is capable of increasing local density of optical states (LDOS) results in the enhanced spontaneous emission rate through the Purcell effect.[3–8] In the past decade, the main focus of the Purcell enhancement has been placed on the manipulation of an electric dipole transition, and less attention has been paid to that of the magnetic dipole and higher order optical transitions. The exact expression of the light-matter interaction Hamiltonian in photoexcitation and relaxation processes is written using a multipolar expansion of the electric (E) and magnetic field (B) as,[9]

$$\mathcal{H} = -\boldsymbol{p} \cdot E - \boldsymbol{m} \cdot B - [\boldsymbol{q}\, \nabla] \cdot E \ldots \quad , \qquad (1)$$

where $\boldsymbol{p}$, $\boldsymbol{m}$ and $\boldsymbol{q}$ are electric dipole, magnetic dipole and electric quadrupole (a tensor) moments, respectively. An optical transition due to the second term, that is the magnetic dipole transition, is usually orders of magnitude weaker than that of the first term; only when electric dipole transitions are forbidden, the second term dominates an emission process. Similar to the Purcell effect on the electric dipole transitions, magnetic dipole transitions can also be manipulated by the local photonic environments (*i.e.*, magnetic Purcell effect). Optical cavities such as metallic mirrors[10,11] and plasmonic nanostructures having magnetic resonances[12–14] are proposed as a structure to manipulate magnetic dipole transitions of rare earth ions (Eu^{3+} and Er^{3+}). However, inherent absorption losses of noble metals in the visible range lead to serious quenching of the emitters nearby and thus the enhancement of the magnetic dipole transitions is limited.

As a new route to circumvent this issue, Mie-type dielectric nanoantennas have been attracting much attention. It is well-known that high refractive index dielectric nanostructures with the size

~ 100 nm or larger exhibit electric and magnetic multipolar Mie resonances at the optical frequency.[15–19] They work not only as a low-loss resonator for the electric Purcell enhancement,[20–22] but also for the magnetic Purcell enhancement.[23–26] Several groups have been succeeded in demonstrating manipulation of magnetic dipole transitions by silicon (Si)-based Mie resonators. In a pioneering work by Sanz-Paz et al,[23] the branching ratio of the magnetic dipole transition ($^5D_0$-$^7F_1$, ~590 nm) to the electric dipole transition ($^5D_0$-$^7F_2$, ~610 nm) of Eu^{3+} is modified by a Si nanoantenna attached to a tip of a scanning probe microscope. However, the observed branching ratio enhancement was marginal (~2). Wiecha et al.[25] investigated Si nanorod dimers covered with a Eu^{3+} doped thin film and observed nearly twice enhancement of the magnetic dipole emission intensity with respect to the electric dipole one. Vaskin et al.[24] also studied the intensity ratio of the magnetic to electric dipole transitions of Eu^{3+} placed on a nanocylinder array made from hydrogenated amorphous Si and observed the increase of ~10%. In all these previous works, the observed magnetic Purcell enhancement is very small. A possible reason for the marginal enhancement is low performance of a nanoantenna in terms of material losses.[24] Furthermore, magnetic dipole emitters are not placed at optimal positions and magnetic Purcell enhancement is smeared through spatial averaging of emission from different positions.[25]

In order to achieve substantial magnetic Purcell enhancement, in this work, we propose a composite system in which Eu^{3+}-based emitters are integrated in a Si nanosphere (NS) antenna (Figure 1). In 2012 Schmidt et al.[27] and Rolly et al.[28] predicted that a Si NS can be an excellent nanoantenna for magnetic Purcell enhancement. However, the experimental proof has not been reported. In this paper, we first study the radiative rate of a magnetic dipole moment longitudinally or transversely coupled to a Si NS antenna by analytical calculations, and demonstrate a large radiative rate enhancement at the magnetic dipole (MD) and magnetic quadrupole (MQ) resonance

frequencies. In order to harness the full potential of a Si NS nanoantenna for magnetic Purcell enhancement, a high-quality crystalline Si NS and a technology to place magnetic dipole emitters at optimal positions near a NS are indispensable. Recently, several methods have been developed to produced crystalline Si NSs.[29,30] In this work, we employ colloidal Si NSs with high crystallinity and sphericity recently developed in our group as a starting material.[31] By taking advantage of colloidal dispersion, we decorate the surface of Si NSs by a monolayer of Eu^{3+} complex molecules (Si NS:Eu) by a wet chemical process. From single particle scattering and photoluminescence (PL) spectroscopy, we show that the PL intensity ratio of the magnetic dipole transition ($^5D_0$-$^7F_1$, ~590 nm) to the electric dipole transition ($^5D_0$-$^7F_2$, ~610 nm) of Eu^{3+} is an order of magnitude enhanced when the MQ resonance of a Si NS is tuned to the magnetic dipole transition wavelength. We also show that the magnetic Purcell enhancement is clearly visible in an ensemble of Si NSs with size distribution.

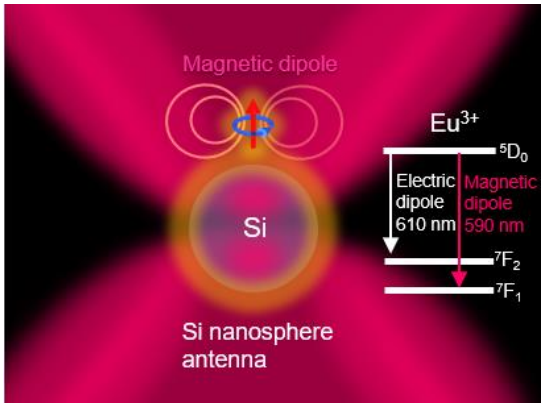

Figure 1. Schematic illustration of magnetic dipole emission of Eu^{3+} coupled to a Si NS antenna.

We first study the radiative decay rate of a magnetic dipole coupled to a Si NS antenna by using analytical formula presented in literature.[27] Figure 2a shows the scattering spectrum of a Si NS (208 nm in diameter) placed in vacuum (n = 1) under plan wave illumination. We see the MD, ED

and MQ resonances in the spectral range. The diameter of a Si NS is chosen so that the MQ resonance overlaps with the magnetic dipole transition ($^5D_0$-$^7F_1$) of Eu^{3+} at 590 nm. Figure 2b shows the radiative ($\Gamma_{\perp rad}/\Gamma_0$) and nonradiative decay rates ($\Gamma_{\perp nonrad}/\Gamma_0$) of a magnetic dipole longitudinally-coupled to a Si NS normalized by the decay rate in vacuum (Γ_0). The distance from the surface of a Si NS is 5 nm which mimics the experiments shown later. We can see significant enhancement of the radiative rate at the MD (795 nm) and MQ (590 nm) resonances. At the MQ resonance wavelength, the enhancement factor reaches 50. At the wavelength, the nonradiative rate is also strongly enhanced due to the non-negligible losses of crystalline Si in the visible range. This decreases the antenna efficiency defined by $\Gamma_{\perp rad}/\Gamma_0/(\Gamma_{\perp rad}/\Gamma_0 + \Gamma_{\perp nonrad}/\Gamma_0)$ to approximately 50%. Note that this antenna efficiency is still higher than those of NSs of previously studied materials such as Ag, Au and amorphous Si (see Figure S1 in the Supporting Information). Figure 2d shows a simulated 3D far-field radiation pattern of a magnetic dipole longitudinally-coupled to a Si NS at the MQ wavelength in Fig. 2b. The associated two-lobe radiation pattern is a characteristic feature of a longitudinal quadrupole mode.[32]

Figure 2c shows the normalized radiative ($\Gamma_{//rad}/\Gamma_0$) and nonradiative ($\Gamma_{//nonrad}/\Gamma_0$) decay rates in the case of transverse coupling. Although weaker than the case of longitudinal coupling, the radiative rate is enhanced at the MD and MQ resonances. The corresponding far-field pattern at the MQ wavelength is shown in Fig. 2e, demonstrating the excitation of a transverse MQ mode.[32] One notices that, in the transverse coupling case, the magnetic dipole moment couples not only to the magnetic resonances but also to the ED resonance of a Si NS. This is due to the presence of the electric field component perpendicular to the Si NS surface. In fact, Mie coefficients corresponding to both the electric and magnetic modes are involved in the analytical formula in the transverse coupling.[27]

By averaging over the dipole orientations, *i.e.*,$(\Gamma_{\perp rad} + 2\Gamma_{//rad})/3\Gamma_0$, the radiative rate for an isotropic dipole is obtained. Figure 2f compares the radiative rate between an isotropic magnetic dipole and an isotropic electric dipole coupled to a 208 nm Si NS. The radiative rate of an isotropic magnetic dipole is enhanced by a factor of 16 and 23 at MD (795 nm) and MQ (590 nm) resonances, respectively. These values are much larger than those of an isotropic electric dipole, *i.e.*, 8.5 and 5 at MD (795 nm) and MQ (590 nm) resonances, respectively. Therefore, strong enhancement of the magnetic dipole emission at 590 nm and strong modification of the branching ratio between the magnetic dipole and electric dipole transitions are expected in a Si-NS:Eu system.

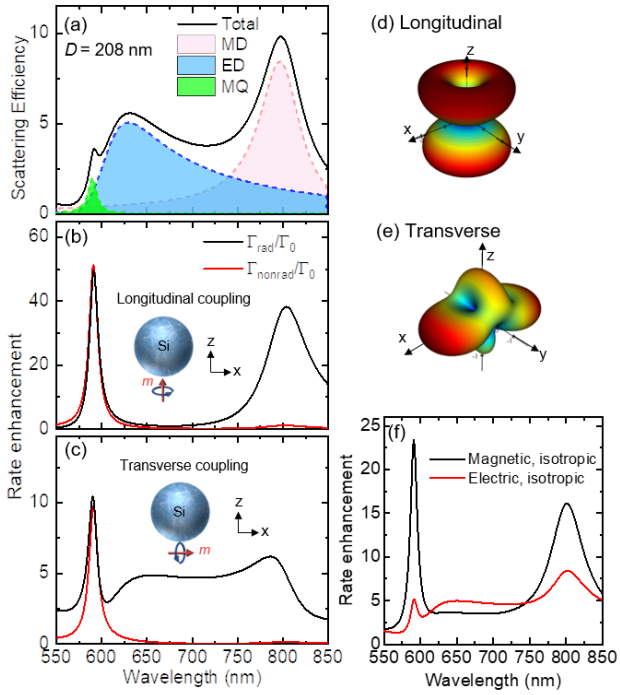

Figure 2. (a) Calculated scattering spectrum of a 208 nm Si NS under plane wave illumination. Contributions of the MD, ED and MQ resonances are also shown. (b,c) Calculated radiative (black curves) and nonradiative (red curves) rate enhancement factors for a magnetic dipole placed 5 nm from the surface of a 208 nm Si NS. (b) longitudinal and (c) transverse coupling geometries. (d, e)

Radiation patterns of (d) longitudinal and (e) transverse coupling geometries at the wavelength of MQ resonance. (f) Radiative rate enhancement factors for an isotropic magnetic dipole (black curve) and an isotropic electric dipole (red curve).

We now move on to the experimental demonstration of the magnetic Purcell enhancement. We prepare crystalline Si NSs with almost perfectly spherical shape by a method reported previously.[31] Figure 3a shows a TEM image of Si NSs. Highly spherical nanoparticles (sphericity >0.95) are obtained. The polydispersity of the diameter distribution is ~35%. As will be shown later and in previous papers,[31,33] the distribution can be reduced to less than 10% by a post-process. A high-resolution image in the inset shows lattice fringes of {111} planes of crystalline Si. Figure 3b shows a measured dark field scattering spectrum (red solid line) of a single Si NS (diameter (D_{Si})= 210 nm). The spectral shape agrees well with the calculated one (black dashed line), evidencing the high sphericity and crystallinity of a Si NS. A slight difference between experiment and calculation is due to the presence of a silica substrate; the ED resonance shifts to longer wavelength and is broadened.[15,34,35]

As a Eu^{3+} emitter, we employ Eu^{3+} complex (Tris(dibenzoylmethane) mono(1,10-phenanthroline)europium(lll)) known as $Eu(DBM)_3$phen. Figure 3c shows a photograph of a $Eu(DBM)_3$phen solution under UV irradiation and the PL spectrum. The emission line at 610 nm is the electric dipole transition ($^5D_0 \rightarrow {}^7F_2$) and that at 590 nm is the magnetic dipole transition ($^5D_0 \rightarrow {}^7F_1$). The branching ratio defined by $\beta_m = I_{590}/(I_{590}+I_{610})$, where I_{590} and I_{610} are emission intensities at 590 nm and 610 nm, respectively, is 0.04. As schematically shown in Figure 3d, $Eu(DBM)_3$phen is attached on the surface of a Si NS via 3-Aminopropyl)trimethoxysilane (APTMS) in a solution (see the Method section). The distance between Si NS surface and a Eu^{3+}

emitter is a sum of the thicknesses of native oxide on Si NS surface (1-2 nm) and a APTMS layer (1-2 nm), and the size of Eu(DBM)3phen molecule (~1 nm). Therefore, the distance may be distributed in a 2-5 nm range. The Si-NS:Eu composites are sparsely deposited on a SiO_2 substrate for single particle spectroscopy.

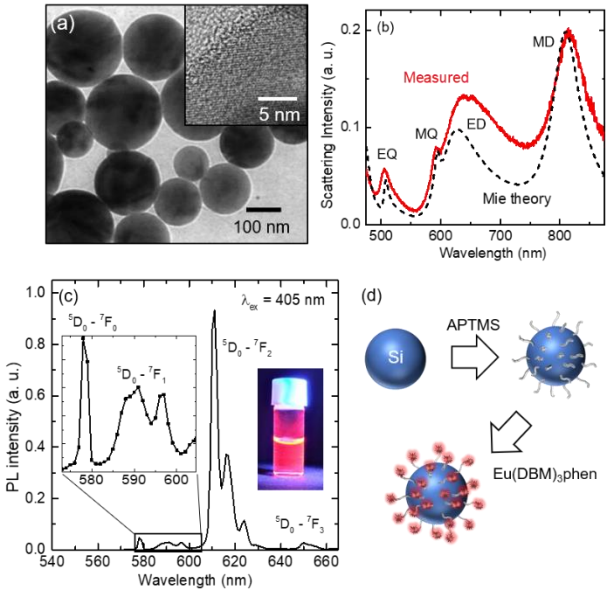

Figure 3. (a) TEM image of colloidal Si NSs. Inset shows a high-resolution TEM image of a Si NS. (b) Measured (red solid line) and calculated (black dashed line) scattering spectra of a 210 nm Si NS. (c) PL spectrum of Eu(DBM)$_3$phen in cyclopentanone. Inset shows a photograph of Eu(DBM)$_3$phen solution under UV irradiation. (d) Schematic of preparation procedure of Si-NS:Eu.

Figure 4a-c shows single particle scattering and PL spectra of Si NS:Eu composites composed of different diameter Si NSs (D_{Si} = 200, 208 and 221 nm). On the measured scattering spectra (upper panel), calculated spectra are overlapped (gray shade). We can see overall agreement

between the measured and calculated spectra. The slight difference arises from the presence of a silica substrate in experiments.[15,35] The vertical broken lines represent the resonance wavelength of a MQ mode. In the lower graphs, PL spectra of Si NS:Eu composites (red line) are shown together with that of $Eu(DBM)_3$phen adsorbed on an APTMS-coated silica substrate (reference, pink shade). The reference PL spectrum is used to estimate the PL enhancement factor in a Si NS:Eu system. We can see that the PL spectral shape is strongly modified by the formation of Si NS:Eu and is very sensitive to the size of a Si NS; small difference of the size results in significant difference in the intensity ratio of the 590 nm to 610 nm peaks. By comparing the PL and scattering spectra, it is obvious that the magnetic dipole transition at 590 nm is strongly enhanced when the MQ resonance of a Si NS approaches the wavelength. To our knowledge, this is the first direct observation of clear spectral modification by the magnetic Purcell effect in dielectric nanoantennas. The difference in the spectral shape is large enough to be recognized as an emission color change in a chromaticity diagram (see Figure S2 in the Supporting Information).

We perform the same experiments for 16 single Si NS:Eu composites and record the PL intensity of the magnetic dipole (I_{590}) and electric dipole (I_{610}) transitions. Some of the PL spectra are shown in the Supporting Information (Figure S3). We then estimate the enhancement factors ($G_{590} = I_{590}/I_{590_ref}$ and $G_{610} = I_{610}/I_{610_ref}$) with respect to the PL intensities of the reference (I_{590_ref} and I_{610_ref}). The ratio of the enhancement factors (G_{590}/G_{610}) is often used as a figure of merit to represent the magnetic Purcell enhancement.[24] Figure 4d shows G_{590}/G_{610} as a function of a Si NS diameter. The G_{590}/G_{610} has a clear peak at D_{Si}~208 nm. In the same figure, a calculated radiative rate enhancement factor of an isotropic magnetic dipole placed 5 nm from NS surface is shown (right axis). Radiative rate enhancement factors for different NS surface-dipole distances (2-5 nm) are shown in the Supporting Information (Figure S4). The radiative rate enhancement at D_{Si}~208

nm is due to the MQ resonance and that at D_{Si}~140 nm due to the MD resonance. We can see that G_{590}/G_{610} is significantly enhanced at the MQ resonance, while the enhancement at the MD resonance is marginal. The enhancement factor is determined by the interplay between the effective mode volume and the Q-factor of resonance modes and the absorption loss of Si. In Figure S5 in the Supporting Information, we show the radiative rate enhancement factors for Si NSs 120-400 nm in diameters. The data indicate that at 590 nm, the MQ mode is the optimal mode for the magnetic Purcell enhancement in a Si NS antenna. In Figure 4d, a remarkable fact is that G_{590}/G_{610} reaches around 11 for 208 nm Si NS, which is an order of magnitude larger than the previously reported value (~1.1) in amorphous Si nanocylinder metasurfaces.[24]

Another important figure of merit of the magnetic Purcell enhancement is the branching ratio between the 610 and 590 nm emissions, since both of them stem from the same excited state of Eu^{3+} ($^5D_0$). If we consider only the $^5D_0$-$^7F_1$ magnetic dipole transition (590 nm) and the $^5D_0$-$^7F_2$ electric dipole transition (610 nm) and ignore other weak $^5D_0$-^7F_n (n = 0, 3-6) transitions, the experimental branching ratio of the magnetic dipole transition (β_{m_exp}) is defined as $\beta_{m_exp} = I_{590}/(I_{590}+I_{610})$. Figure 4e plots β_{m_exp} as a function of a Si NS diameter. The horizontal dashed line is the branching ratio obtained for a reference sample. We can see a clear peak of the branching ratio at D_{Si}~208 nm. The gain is at maximum ~7. Again, this gain is much larger than the reported highest value in dielectric nanostructures (~2).[23,25]

The branching ratio can be calculated as,[10]

$$\beta_{\mathrm{m}} = \frac{\beta_{\mathrm{m}}^{\mathrm{ref}}\rho_{\mathrm{m}}}{\beta_{\mathrm{m}}^{\mathrm{ref}}\rho_{\mathrm{m}}+\beta_{\mathrm{e}}^{\mathrm{ref}}\rho_{\mathrm{e}}} \ , \qquad (2)$$

where $\beta_{\mathrm{e}}^{\mathrm{ref}}$ and $\beta_{\mathrm{m}}^{\mathrm{ref}}$ are the branching ratios of electric and magnetic dipole transitions, respectively, of a reference sample, and ρ_{e} and ρ_{m} are radiative rate enhancement factors (Γ_{rad}/Γ_0) for isotropic electric (610 nm) and magnetic (590 nm) dipoles, respectively, discussed in Fig. 2.

The calculated branching ratio is shown in Figure 4e by a red curve. We can see very good agreement between the experimental and calculated branching ratios. Interestingly, the experimental branching ratio at 208 nm is larger than the calculated one. The slight discrepancy may arise from the presence of a silica substrate in experiments; a silica substrate shifts the electric dipole mode to longer wavelength, which reduces ρ_e at 610 nm, and makes β_m slightly larger.

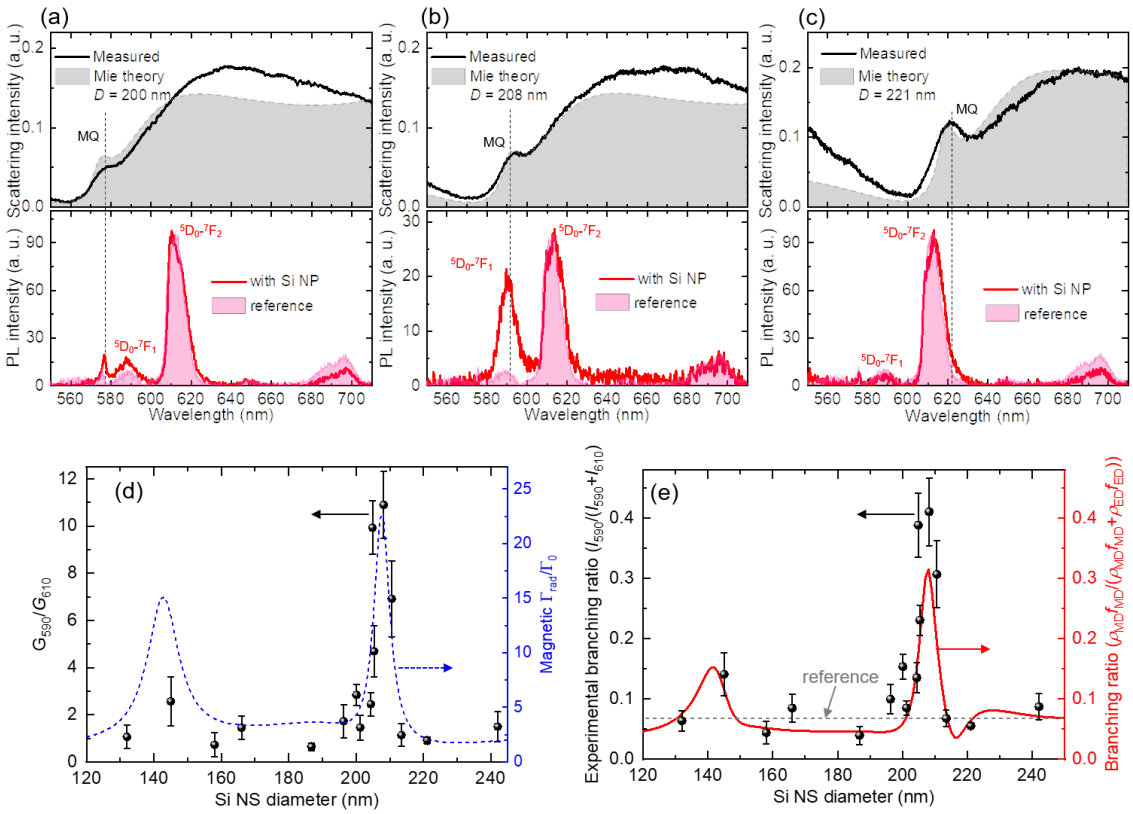

Figure 4. (a-c) Scattering (upper panels) and PL spectra (bottom panels) of single Si NS:Eu particles with different diameters ((a) 200, (b) 208 and (c) 221 nm). Gray and pink shaded spectra are calculated scattering and PL spectra of a reference sample, respectively. (d) The ratio of the enhancement factors of the 590 nm peak to the 610 nm peak (G_{590}/G_{610}) (black dots), and calculated radiative rate enhancement factor of an isotropic magnetic dipole moment placed 5 nm from NP surface (Γ_{rad}/Γ_0) (blue curve) as a function of a Si NS diameter. (e) Experimental (black

dots) and calculated (red curve) branching ratios of the magnetic dipole transition at 590 nm as a function of a Si NS diameter.

Following the single NS study, we extend the work to an ensemble of Si NSs. As shown in Figure 4a-c, the magnetic Purcell enhancement is very sensitive to the size of a Si NS. Therefore, small size distribution easily smears the effect, and thus the size purification is crucial to obtain magnetic Purcell enhancement in a macroscopic scale. Figure 5a shows extinction spectra of as-prepared and size-purified Si NSs before conjugation with $Eu(DBM)_3$phen. Distinctive peaks similar to a single particle scattering spectrum appears after the size purification even in the solution with a higher refractive index than air. The TEM image of a size-purified sample in the inset shows very uniform size NSs. The average diameter and the standard deviation (σ) obtained from TEM images are 208 nm and 7.6%, respectively (see Figure S5 in the Supporting Information). Figure 5b and c show dark field scattering images of as-prepared and size-purified NSs deposited on a silica substrate, demonstrating that NSs with blue and green scattering colors are removed by the purification process. Figure 5d shows a PL spectrum of size-purified Si NS:Eu particles on a substrate. The PL is obtained for ~1 mm diameter excitation spot, which contains >70,000 Si NS:Eu particles. We can see the enhancement of the branching ratio compared to the reference; the branching ratio (β_m) is 0.10 ± 0.01, which is enhanced by a factor of 1.9 with respect to the reference. Although this value is smaller than that obtained in single NS spectroscopy in Fig. 4, it is larger than that of previous work.[24] In the ensemble, we also measure the PL lifetime (Figure S7 and Table S1 in the Supporting Information) and observe the reduction by the formation of Si NS:Eu.

In order to see the validity of the branching ratio obtained for the Si NS:Eu composite ensemble, we calculate the radiative rate enhancement factors for isolated electric (ρ_e) and magnetic (ρ_m) dipoles by taking into account the size distribution. The results are shown in Figure 5e as a function of wavelength. Compared to the data obtained for a single NS in Figure 2f, the peaks are broadened and the enhancement factors are largely reduced. However, we still see that ρ_m at 590 nm ($^5D_0$-$^7F_1$) is larger than ρ_e at 610 nm ($^5D_0$-$^7F_2$), and thus the increase of the branching ratio (β_m in eq.(2)) is expected. The calculated branching ratio is 0.09, which is close to that obtained in the experiment.

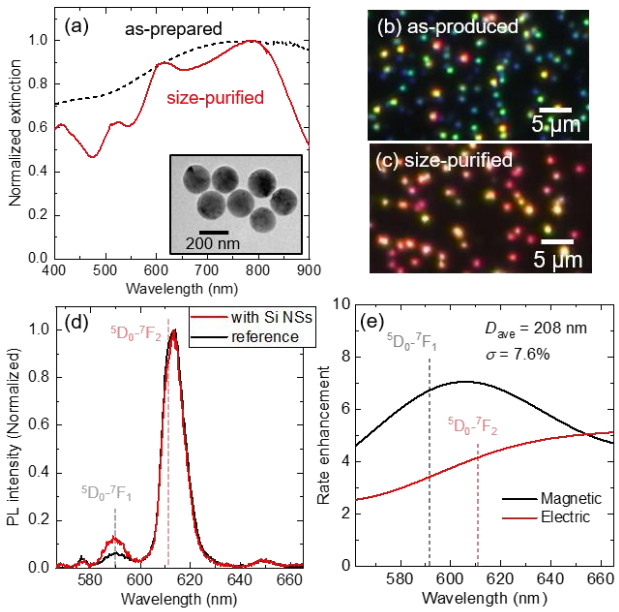

Figure 5. (a) Normalized extinction spectra of as-prepared and size-purified Si NSs in solution. Inset: TEM image of size-purified Si NSs. Dark field microscope images of (b) as-prepared and (c) size-purified Si NSs on silica substrates. (d) Normalized PL spectra of Si NS:Eu composite ensemble on silica substrate (red curve) and that of a reference sample (black curve). (e) Calculated

radiative rate enhancement factors of electric and magnetic dipoles when size distribution is taken into account. The average diameter is 208 nm and the standard deviation is 7.6%.

In summary, we have achieved a large enhancement of the magnetic dipole emission of Eu^{3+} emitters by the magnetic Purcell effect induced by a spherical Si nanoantenna. The enhancement factor of the branching ratio between the magnetic and electric dipole transitions reaches ~7 when the MQ resonance of a Si NS is overlapped on the magnetic dipole transition of Eu^{3+}. The enhancement results in strong modification of the Eu^{3+} emission spectrum, which can be recognized as a color change. Observed size dependence of the branching ratio agrees very well with calculated ones. The size dependence provided clear evidence that observed spectral modification arises from the magnetic Purcell effect. We also demonstrated that the magnetic Purcell enhancement is observable in ensemble of Si NS:Eu composites even if there is size distribution. The observed magnetic Purcell enhancement driven by colloidal Mie resonators offers an opportunity not only to develop novel fluorophores with enhanced magnetic dipole emission, but also to control the excited state of the matter in photochemistry.

Methods

Calculation of decay rates of electric and magnetic dipoles near Si nanospheres: The analytical expressions for the calculation of radiative and total decay rate enhancement factors of electric and magnetic dipoles in the vicinity of a sphere are obtained from literatures.[27,36] Briefly, the dipolar electromagnetic field written as a series of vector spherical harmonics and the scattered field by a sphere were calculated by Mie theory.[37] By integrating the Poynting vector over the full solid angles in the far-field, total radiated power (i.e., radiative rate) was calculated. Nonradiative loss was calculated by integrating the energy inflow over all the absorbing region (i. e., inside a sphere).

For the calculations, the complex dielectric permittivity of crystalline Si taken from a literature[38] was used. The 3D radiation patterns in Fig. 2d and e were calculated using a finite-difference time-domain method using a commercial software (Ansys Lumerical FDTD).

Preparation of colloidal dispersion of size-separated Si nanospheres: Si NSs were prepared by thermal disproportionation of SiO. SiO lumps (several mm in size) (Wako, 99.9%) were crushed to powder and annealed at 1475°C in a N_2 gas atmosphere for 30 min to grow crystalline Si NSs in SiO_2 matrices. Si NSs were liberated from SiO_2 matrices by etching in HF solution (46 wt.%) for 1 h. Liberated NSs were then transferred to methanol and subsequently subjected to a minute sonication with an ultrasonic homogenizer (Violamo SONICSTAR 85). Size separation of Si NSs was made by a density gradient centrifugation method. Briefly, sucrose density gradient solutions were prepared by carefully adding sucrose solutions at three different concentrations (45, 42.5, and 40 wt.%) to a centrifugal tube in order. Colloidal dispersion of Si NSs was added to the top of the tube, and it was the subject of centrifugation at 4000 rpm for 25 min to form layers of size-separated Si NSs. The layers were retrieved from the top and transferred to different vials. The solutions of size-separated Si NSs were washed with water several times to remove sucrose.

To prepare Si-NS:Eu, the surface of Si NSs was first functionalized with 3-Aminopropyl)trimethoxysilane (APTMS) in methanol. After removing excess APTMS by centrifugation, NSs were mixed with $Eu(DBM)_3$phen solution and stirred. During stirring, $Eu(DBM)_3$phen was unspecifically bound to APTMS-functionalized Si NSs. The Si NS:Eu composites were washed more than 3 times to completely remove unbound $Eu(DBM)_3$phen and were deposited on a SiO_2 substrate for the spectroscopic study.

Optical microspectroscopy of single Si nanospheres: A custom-built inverted optical microscope was used for dark-field backward scattering and PL measurements of single Si NS:Eu particles. For the scattering measurement, a sample was placed facedown onto the stage and illuminated by a halogen lamp through a dark-field objective lens (100×, NA = 0.9), and the scattered light was collected by the same objective lens. To measure the spectra, the scattered light was transferred to the entrance slit of a monochromator (SpectraPro-300i, Acton Research Corp.) and detected by a liquid-N_2 cooled CCD (Princeton Instruments). For the PL measurement, a Si NS:Eu was excited by 405 nm light *via* the objective lens. The power density at the sample was reduce to <1 W/cm^2 to avoid local heating and degradation of Eu(DBM)$_3$phen.

ASSOCIATED CONTENT

This material is available free of charge via the internet at http://pubs.acs.org.

Additional experimental data including emission spectra, chromaticity diagram and PL decay curves, additional calculation data of decay rate enhancement for different materials and radiative rate enhancement (PDF).

Corresponding Author

*sugimoto@eedept.kobe-u.ac.jp

ACKNOWLEDGMENT

H.S. acknowledges the support provided by JST, PRESTO Grant number JPMJPR19T4.

REFERENCES

(1) Giannini, V.; Fernández-Domínguez, A. I.; Heck, S. C.; Maier, S. a. Plasmonic Nanoantennas: Fundamentals and Their Use in Controlling the Radiative Properties of Nanoemitters. *Chem. Rev.* **2011**, *111*, 3888–3912. https://doi.org/10.1021/cr1002672.

(2) Novotny, L.; Hecht, B. *Principles of Nano-Optics*; Cambridge University Press: Cambridge, 2006. https://doi.org/10.1017/CBO9780511813535.

(3) Akselrod, G. M.; Argyropoulos, C.; Hoang, T. B.; Ciracì, C.; Fang, C.; Huang, J.; Smith, D. R.; Mikkelsen, M. H. Probing the Mechanisms of Large Purcell Enhancement in Plasmonic Nanoantennas. *Nat. Photonics* **2014**, *8* (11), 835–840. https://doi.org/10.1038/nphoton.2014.228.

(4) Lu, D.; Kan, J. J.; Fullerton, E. E.; Liu, Z. Enhancing Spontaneous Emission Rates of Molecules Using Nanopatterned Multilayer Hyperbolic Metamaterials. *Nat. Nanotechnol.* **2014**, *9* (1), 48–53. https://doi.org/10.1038/nnano.2013.276.

(5) Kinkhabwala, A.; Yu, Z.; Fan, S.; Avlasevich, Y.; Müllen, K.; Moerner, W. E. Large Single-Molecule Fluorescence Enhancements Produced by a Bowtie Nanoantenna. *Nat. Photonics* **2009**, *3* (11), 654–657. https://doi.org/10.1038/nphoton.2009.187.

(6) Cambiasso, J.; Grinblat, G.; Li, Y.; Rakovich, A.; Cortés, E.; Maier, S. A. Bridging the Gap between Dielectric Nanophotonics and the Visible Regime with Effectively Lossless Gallium Phosphide Antennas. *Nano Lett.* **2017**, *17* (2), 1219–1225. https://doi.org/10.1021/acs.nanolett.6b05026.

(7) Kuznetsov, A. I.; Miroshnichenko, A. E.; Brongersma, M. L.; Kivshar, Y. S.; Luk'yanchuk, B. Optically Resonant Dielectric Nanostructures. *Science (80-.).* **2016**, *354* (6314), aag2472. https://doi.org/10.1126/science.aag2472.

(8) Bidault, S.; Mivelle, M.; Bonod, N. Dielectric Nanoantennas to Manipulate Solid-State Light Emission. *J. Appl. Phys.* **2019**, *126* (9). https://doi.org/10.1063/1.5108641.

(9) Kasperczyk, M.; Person, S.; Ananias, D.; Carlos, L. D.; Novotny, L. Excitation of Magnetic Dipole Transitions at Optical Frequencies. *Phys. Rev. Lett.* **2015**, *114* (16), 163903. https://doi.org/10.1103/PhysRevLett.114.163903.

(10) Aigouy, L.; Cazé, A.; Gredin, P.; Mortier, M.; Carminati, R. Mapping and Quantifying Electric and Magnetic Dipole Luminescence at the Nanoscale. *Phys. Rev. Lett.* **2014**, *113* (7), 1–5. https://doi.org/10.1103/PhysRevLett.113.076101.

(11) Rabouw, F. T.; Prins, P. T.; Norris, D. J. Europium-Doped NaYF4 Nanocrystals as Probes for the Electric and Magnetic Local Density of Optical States throughout the Visible Spectral Range. *Nano Lett.* **2016**, *16* (11), 7254–7260. https://doi.org/10.1021/acs.nanolett.6b03730.

(12) Ernandes, C.; Lin, H. J.; Mortier, M.; Gredin, P.; Mivelle, M.; Aigouy, L. Exploring the Magnetic and Electric Side of Light through Plasmonic Nanocavities. *Nano Lett.* **2018**, *18* (8), 5098–5103. https://doi.org/10.1021/acs.nanolett.8b01956.

(13) Hussain, R.; Kruk, S. S.; Bonner, C. E.; Noginov, M. A.; Staude, I.; Kivshar, Y. S.; Noginova, N.; Neshev, D. N. Enhancing Eu^3+ Magnetic Dipole Emission by Resonant Plasmonic Nanostructures. *Opt. Lett.* **2015**. https://doi.org/10.1364/ol.40.001659.

(14) Choi, B.; Iwanaga, M.; Sugimoto, Y.; Sakoda, K.; Miyazaki, H. T. Selective Plasmonic Enhancement of Electric- and Magnetic-Dipole Radiations of Er Ions. *Nano Lett.* **2016**, *16* (8), 5191–5196. https://doi.org/10.1021/acs.nanolett.6b02200.

(15) Kuznetsov, A. I.; Miroshnichenko, A. E.; Fu, Y. H.; Zhang, J.; Luk'yanchuk, B. Magnetic Light. *Sci. Rep.* **2012**, *2* (1), 492. https://doi.org/10.1038/srep00492.

(16) Fu, Y. H.; Kuznetsov, A. I.; Miroshnichenko, A. E.; Yu, Y. F.; Luk'yanchuk, B. Directional Visible Light Scattering by Silicon Nanoparticles. *Nat. Commun.* **2013**, *4*, 1527. https://doi.org/10.1038/ncomms2538.

(17) Evlyukhin, A. B.; Novikov, S. M.; Zywietz, U.; Eriksen, R. L.; Reinhardt, C.; Bozhevolnyi, S. I.; Chichkov, B. N. Demonstration of Magnetic Dipole Resonances of Dielectric Nanospheres in the Visible Region. *Nano Lett.* **2012**, *12* (7), 3749–3755. https://doi.org/10.1021/nl301594s.

(18) Evlyukhin, A. B.; Reinhardt, C.; Seidel, A.; Luk'yanchuk, B. S.; Chichkov, B. N. Optical Response Features of Si-Nanoparticle Arrays. *Phys. Rev. B* **2010**, *82* (4), 045404. https://doi.org/10.1103/PhysRevB.82.045404.

(19) García-Etxarri, A.; Gómez-Medina, R.; Froufe-Pérez, L. S.; López, C.; Chantada, L.; Scheffold, F.; Aizpurua, J.; Nieto-Vesperinas, M.; Sáenz, J. J. Strong Magnetic Response of Submicron Silicon Particles in the Infrared. *Opt. Express* **2011**, *19* (6), 4815–4826. https://doi.org/10.1364/OE.19.004815.

(20) Caldarola, M.; Albella, P.; Cortés, E.; Rahmani, M.; Roschuk, T.; Grinblat, G.; Oulton, R. F.; Bragas, A. V; Maier, S. A. Non-Plasmonic Nanoantennas for Surface Enhanced

Spectroscopies with Ultra-Low Heat Conversion. *Nat. Commun.* **2015**, *6*, 7915. https://doi.org/10.1038/ncomms8915.

(21) Sugimoto, H.; Fujii, M. Colloidal Dispersion of Subquarter Micrometer Silicon Spheres for Low-Loss Antenna in Visible Regime. *Adv. Opt. Mater.* **2017**, *5* (17), 1700332. https://doi.org/10.1002/adom.201700332.

(22) Krasnok, A.; Caldarola, M.; Bonod, N.; Alú, A. Spectroscopy and Biosensing with Optically Resonant Dielectric Nanostructures. *Adv. Opt. Mater.* **2018**, *6* (5), 1701094. https://doi.org/10.1002/adom.201701094.

(23) Sanz-Paz, M.; Ernandes, C.; Esparza, J. U.; Burr, G. W.; van Hulst, N. F.; Maitre, A.; Aigouy, L.; Gacoin, T.; Bonod, N.; Garcia-Parajo, M. F.; Bidault, S.; Mivelle, M. Enhancing Magnetic Light Emission with All-Dielectric Optical Nanoantennas. *Nano Lett.* **2018**, *18* (6), 3481–3487. https://doi.org/10.1021/acs.nanolett.8b00548.

(24) Vaskin, A.; Mashhadi, S.; Steinert, M.; Chong, K. E.; Keene, D.; Nanz, S.; Abass, A.; Rusak, E.; Choi, D.-Y.; Fernandez-Corbaton, I.; Pertsch, T.; Rockstuhl, C.; Noginov, M. A.; Kivshar, Y. S.; Neshev, D. N.; Noginova, N.; Staude, I. Manipulation of Magnetic Dipole Emission from Eu 3+ with Mie-Resonant Dielectric Metasurfaces. *Nano Lett.* **2019**, *19* (2), 1015–1022. https://doi.org/10.1021/acs.nanolett.8b04268.

(25) Wiecha, P. R.; Majorel, C.; Girard, C.; Arbouet, A.; Masenelli, B.; Boisron, O.; Lecestre, A.; Larrieu, G.; Paillard, V.; Cuche, A. Enhancement of Electric and Magnetic Dipole Transition of Rare-Earth-Doped Thin Films Tailored by High-Index Dielectric Nanostructures. *Appl. Opt.* **2019**, *58* (7), 1682. https://doi.org/10.1364/AO.58.001682.

(26) Cheng, X.; Zhuo, X.; Jiang, R.; Wang, Z.; Wang, J.; Lin, H. Electromagnetic Resonance-Modulated Magnetic Emission in Europium-Doped Sub-Micrometer Zirconia Spheres. *Adv. Opt. Mater.* **2021**, *2002212*, 2002212. https://doi.org/10.1002/adom.202002212.

(27) Schmidt, M. K.; Esteban, R.; Sáenz, J. J.; Suárez-Lacalle, I.; Mackowski, S.; Aizpurua, J. Dielectric Antennas - a Suitable Platform for Controlling Magnetic Dipolar Emission: Errata. *Opt. Express* **2012**, *20* (17), 18609. https://doi.org/10.1364/oe.20.018609.

(28) Rolly, B.; Bebey, B.; Bidault, S.; Stout, B.; Bonod, N. Promoting Magnetic Dipolar Transition in Trivalent Lanthanide Ions with Lossless Mie Resonances. *Phys. Rev. B - Condens. Matter Mater. Phys.* **2012**, *85* (24), 2–7. https://doi.org/10.1103/PhysRevB.85.245432.

(29) Zywietz, U.; Evlyukhin, A. B.; Reinhardt, C.; Chichkov, B. N. Laser Printing of Silicon Nanoparticles with Resonant Optical Electric and Magnetic Responses. *Nat. Commun.* **2014**, *5*, 3402. https://doi.org/10.1038/ncomms4402.

(30) Garín, M.; Solà, M.; Julian, A.; Ortega, P. Enabling Silicon-on-Silicon Photonics with Pedestalled Mie Resonators. *Nanoscale* **2018**, *10* (30), 14406–14413. https://doi.org/10.1039/C8NR02259C.

(31) Sugimoto, H.; Okazaki, T.; Fujii, M. Mie Resonator Color Inks of Monodispersed and Perfectly Spherical Crystalline Silicon Nanoparticles. *Adv. Opt. Mater.* **2020**, *8* (12), 2000033. https://doi.org/10.1002/adom.202000033.

(32) Das, T.; Iyer, P. P.; DeCrescent, R. A.; Schuller, J. A. Beam Engineering for Selective and Enhanced Coupling to Multipolar Resonances. *Phys. Rev. B* **2015**, *92* (24), 241110. https://doi.org/10.1103/PhysRevB.92.241110.

(33) Hinamoto, T.; Hotta, S.; Sugimoto, H.; Fujii, M. Colloidal Solutions of Silicon Nanospheres toward All-Dielectric Optical Metafluids. *Nano Lett.* **2020**, *20* (10), 7737–7743. https://doi.org/10.1021/acs.nanolett.0c03295.

(34) Kuo, Y.-L.; Chuang, S.-Y.; Chen, S.-Y.; Chen, K.-P. Enhancing the Interaction between High-Refractive Index Nanoparticles and Gold Film Substrates Based on Oblique Incidence Excitation. *ACS Omega* **2016**, *1* (4), 613–619. https://doi.org/10.1021/acsomega.6b00105.

(35) Sugimoto, H.; Hinamoto, T.; Fujii, M. Forward to Backward Scattering Ratio of Dielectric–Metal Heterodimer Suspended in Almost Free-Space. *Adv. Opt. Mater.* **2019**, *7* (20), 1900591. https://doi.org/10.1002/adom.201900591.

(36) Ruppin, R. Decay of an Excited Molecule near a Small Metal Sphere. *J. Chem. Phys.* **1982**. https://doi.org/10.1063/1.443196.

(37) Bohren, C. F.; Huffman, D. R. *Absorption and Scattering of Light by Small Particles*; John Wiley & Sons, 1983. https://doi.org/10.1002/9783527618156

(38) Palik, E. D. *Handbook of Optical Constants of Solids*; Academic press, 1998; Vol. 3. ISBN: 9780080533780

For Table of Contents Use Only

Magnetic Purcell Enhancement by Magnetic Quadrupole Resonance of Dielectric Nanosphere Antenna
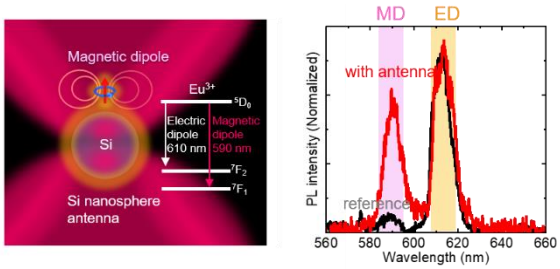
Hiroshi Sugimoto, and Minoru Fujii